Synthesis and Spectroscopic Investigations of a Crystalline Humidity Sensor: Bis(triphenylphosphine)iminium 2,2′-Bipyridyltetracyanoruthenate

Jon K. Evju and Kent R. Mann*

Department of Chemistry, University of Minnesota, Minneapolis, Minnesota 55455-0431

Received May 4, 1998. Revised Manuscript Received April 12, 1999

We have prepared a new salt of the solvatochromic $[Ru(bpy)(CN)_4]^{2-}$ anion bis(triphenylphosphine)iminium 2,2′-bipyridyltetracyanoruthenate, $((PPN)_2[Ru(bpy)(CN)_4])$, that reversibly sorbs water and changes color from purple to yellow when it is exposed to humid air. Solid samples of anhydrous $(PPN)_2[Ru(bpy)(CN)_4]$ reversibly hydrate in humid air, first to $(PPN)_2[Ru(bpy)(CN)_4]\cdot H_2O$ and then to $(PPN)_2[Ru(bpy)(CN)_4]\cdot 15H_2O$. A single-crystal X-ray study of $(PPN)_2[Ru(bpy)(CN)_4]\cdot 2CH_3CN\cdot 2(CH_3CH_2)_2O\cdot 2H_2O$ shows that this novel humidity sensor has large channels in the structure that allows sorbed water molecules to reversibly interact with the cyanide ligands of the chromophore. The hydration changes that result from exposure of the solid in the 0 to 66% relative humidity range cause the MLCT visible absorption bands to shift dramatically to higher energy. These hydration changes also result in large shifts in the ν(CN) region of the infrared spectrum; these changes indicate significant H-bonding interactions between sorbed water molecules and the dianionic chromophore occur in the crystal lattice. The hydration changes in the 66 to 100% relative humidity range cause large intensity changes in a visible photoluminescence band. This emission intensity increase is accompanied by small wavelength shifts in absorption and emission and in the ν(CN) region of the infrared spectrum. These changes are consistent with further oligomerization of the water molecules that initially formed hydrogen-bonding interactions to the cyanide ligands.

Introduction

We are interested in the design and study of new solid-state sensor materials that selectively sorb gas-phase solvent molecules.[1−4] The sorption process introduces guest molecules into a carefully designed host crystal lattice that contains a solvatochromic chromophore. Host−guest interactions change the absorption and emission properties of the chromophore and allow the detection and quantification of the guest. Properly designed solid-state sensor materials of this type exhibit vapochromic[5] and vapoluminescent[4] behavior and may be useful components for environmental sensor devices.[6−9]

Among the many analytes with environmental and industrial importance, water has nearly universal interest. Many optical humidity sensors recently reported in the literature are based on mixtures of solvatochromic dyes and water permeable polymers.[10] While these mixed-phase systems may be more than adequate for technological applications, their complexity (i.e., the number of active sites present and a lack of detailed structural information) precludes the elucidation of the most critical design features of the response. Pure crystalline compounds are more attractive for study as model systems because the crystallographically imposed site symmetry allows the shift mechanisms to be studied by X-ray diffraction techniques.[4] To date, only a few pure compounds have been reported that can optically sense water vapor concentrations in air,[4,11] so we directed our work to this area. We began with the intention to use the well-documented solvatochromic diiminetetracyanoruthenate anions[12−24] as a required

* To whom correspondence should be addressed.

(1) Exstrom, C. L.; Sowa, J. R., Jr.; Daws, C. A.; Janzen, D.; Moore, G. A.; Mann, K. R. *Chem. Mater.* **1995**, *7*, 15.
(2) Daws, C. A.; Exstrom, C. L.; Sowa, J. R., Jr.; Mann, K. R. *Chem. Mater.* **1997**, *9*, 363.
(3) Exstrom, C. L.; Pomije, M. K.; Mann, K. R. *Chem. Mater.* **1998**, *10*, 942.
(4) Buss, C. E.; Anderson,C. E.; Pomije, M. K.; Lutz, C. M.; Britton, D.; Mann, K. R. *J. Am. Chem. Soc.* **1998**, *120*, 7783.
(5) Nagel, C. C. U.S. Patent 4,834,909, 1989.
(6) Persaud, K.; Dodd, G. H. *Nature (London)* **1982**, *299*, 352.
(7) Shurmer, H. V. *Anal. Proc. Inc. Anal. Commun.* **1994**, *31*, 39.
(8) Kunugi, Y.; Mann, K. R.; Miller, L. L.; Exstrom, C. L. *J. Am. Chem. Soc.* **1998**, *120*, 589.
(9) Kunugi, Y.; Mann, K. R.; Miller, L. L.; Pomije, M. K. *Chem. Mater.* **1998**, *10*, 1487.
(10) (a) Wang, K.; Seiler, K.; Haug, J.-P.; Lehmann, B.; West, S.; Hartman, K.; Simon, W. *Anal. Chem.* **1991**, *63*, 970. (b) Papkovsky, D. B.; Ponomarev, G. V. Chernov, S. F.; Ovchinnikov, A. N.; Kurochkin, I. N. *Sens. Actuators B* **1994**, *22*, 57. (c) Bearzotti, A.; Amico, A. D.; Furlani, A.; Iucci, G.; Russo, M. V. *Sens. Actuators B* **1992**, *7*, 451. (d) Sadaoka, Y.; Matsguchi, M.; Sakai, Y.; Murata, Y. *Chem. Lett.* **1992**, 53. (e) Krech, J. H. and Rose-Pehrsson, S. L. *Anal. Chim. Acta*. **1997**, *341*, 53. (f) Grate, J. W.; Abraham, M. H. *Sens. Actuators B*, **1991**, *3*, 85. (g) Sabatani, E.; Nikol, H. D.; Gray, H. B.; Anson, F. C. *J. Am. Chem. Soc.* **1996**, *118*, 1158.
(11) (a) Shih, K.-C.; Herber, R. H. *Inorg. Chem.* **1992**, *31*, 5444. (b) Boltinghouse, F.; Abel, K. *Anal. Chem.* **1989**, *61*, 1863.
(12) Chang, Q.; Murtaza, Z.; Lakowicz, J. R.; Rao, G. *Anal. Chim. Acta* **1997**, *350*, 97.

10.1021/cm980323i CCC: $18.00
Published on Web 05/19/1999

structural component. The diiminetetracyanoruthenate anions are very stable and exhibit shifts in the $E°_{red}$, $E°_{ox}$, the UV−vis absorption and the emission spectra that correlate to the Gutmann acceptor number of the solvent used to dissolve the anion.[20,23] For the cation, we chose bis(triphenylphosphine)iminium (PPN^+) as it structurally resembles the "hexa-hosts" that have been investigated previously in inclusion chemistry.[25]

Our design strategy was successful and herein we report a new solid-state sensor compound bis(triphenylphosphine)iminium 2,2′-bipyridyltetracyanoruthenate, $(PPN)_2[Ru(bpy)(CN)_4]\cdot xH_2O$; $x = 0-15$) with variable hydration levels. This salt reversibly sorbs water from air and exhibits shifts in spectroscopic behavior that allow an exploration of the sensing mechanism over the full range of relative humidities (0 to 100%) at ambient temperatures. These observations suggest that the sensor compound is sensitive to the number of water molecules sorbed and their arrangement relative to the chromophore in the solid state.

Experimental Section

General Considerations. Ethanol (95 and 100%) were supplied by AAPER Alcohol and Chemical Co. Other solvents were ACS reagent grade solvents supplied by Mallinckrodt, Fisher, or Aldrich and were used as received. 2,2′-bipyridine was purchased from Aldrich and was used as received. Nitrogen gas, industrial grade, was supplied by Airgas or Air Products and was used as received unless otherwise noted. Bis(triphenylphosphine)iminium chloride (PPNCl) was supplied by Alfa Products and was used as received. η^6-Benzeneruthenium-μ-dichloro dimer, $[BzRuCl_2]_2$,[26] was prepared according to a literature procedure.[27] An improved synthesis of $K_2[Ru(bpy)(CN)_4]$[14] is described below. Elemental analyses were carried out by Quantitative Technologies Incorporated, Whitehouse, NJ. NMR spectra were obtained with Varian VI 300, VXR 300 or VI 500 spectrometers and were referenced to $(CH_3)_4Si$. FT-IR spectra were recorded with a Nicolet Magna 550 infrared spectrophotometer as films on a zinc selenide attenuated total reflectance (ATR) crystal, as films on calcium fluoride or as solutions in a calcium fluoride solution cell as noted.

Materials. *[BzRu(bpy)Cl]Cl.* η^6-Benzene-2,2′-bipyridinechlororuthenium chloride was prepared via a slight modification of the PF_6^- salt synthesis reported by Stephenson et al.[28] A 250-mL flask was charged with 0.926 g (5.93 mmol) of 2,2′-bipyridine and 1.573 g (3.15 mmol) of $[BzRuCl_2]_2$. Ethanol (150 mL of 95%) was added, and the reaction mixture was stirred at room temperature for 14 h. The resulting solution of the chloride salt was filtered and rotoevaporated to dryness. The residue was redissolved in water, filtered, and rotoevaporated to dryness again. After recrystallization from methanol and diethyl ether, 1.990 g (4.90 mmol) of the bright yellow orange chloride salt was isolated (83% yield). ^1H NMR (CD_3CN) (shift (ppm), (multiplicity, J_{HH}, integration): 9.43 (d, 5.7 Hz, 2), 8.33 (d, 7.9 Hz, 2), 8.18 (dd, 7.6 Hz, 2), 7.69 (dd, 6.3 Hz, 2), 6.026 (s, 6).

$K_2[Ru(bpy)(CN)_4]$. A solution of 0.442 g (1.09 mmol) of [BzRu(bpy)Cl]Cl was dissolved in 40 mL of methanol. This solution was slowly added (1 drop per 1−2 s) under a nitrogen purge to a cooled solution of 1.202 g (18.5 mmol) of KCN in 320 mL of methanol in a quartz photochemical reaction well. The reaction mixture was purged with nitrogen and kept at 5−9 °C during photolysis with a 400-W medium-pressure mercury lamp (converted Sylvania type H33 street lamp). After a total of 8 h of photolysis, the reaction was complete, as determined by proton NMR. An insoluble red byproduct was filtered from the orange reaction mixture. The methanol was removed by rotoevaporation. The resulting solid was purified by several recrystallizations from 1:30 water:acetone, 1:40 water:absolute ethanol, and 1:30:100 water:methanol:dichloromethane solvent mixtures. The orange product (0.2294 g, 0.5186 mmol) was isolated to give a 48% yield. The proton NMR spectrum compares well with the literature.[29] ^1H NMR (50:50 D_2O:CD_3OD) (shift (ppm), (multiplicity, J_{HH}, integration):[30] 9.00 (d, 5.4 Hz, 2), 7.83 (d, 8.1 Hz, 2), 7.56 (dd, 8.0 Hz, 2), 7.24 (dd, 5.9 Hz, 2). ^{13}C NMR (50:50 D_2O:CD_3OD) (proton decoupled, shift (ppm)):[30] 164.1, 162.2, 153.9, 151.0, 135.4, 124.3, 120.9. IR (ATR, from 50:50 methanol:water solution, wet): 2091 (w), 2059 (vs), 2046 (s), 2032 (m).

$(PPN)_2[Ru(bpy(CN)_4]\cdot xH_2O$. $K_2[Ru(bpy)(CN)_4]$ (0.390 g, 0.887 mmol), dissolved in 1.5 mL of H_2O, and 1.158 g of PPNCl (2.02 mmol), dissolved in 170 mL of warm H_2O, were combined to give the water-insoluble PPN^+ salt. The orange precipitate was filtered and washed with 100 mL of H_2O. The color of the product changed to red as it dried on the filter frit. After recrystallizing twice from acetonitrile and ether, red violet crystalline product was obtained. The product was dried in vacuo at 111 °C. The product (1.087 g, 0.756 mmol, 85% yield) was obtained. Mp (sealed tube): 238−242 °C. ^1H NMR (CD_2Cl_2) (shift (ppm), (multiplicity, J_{HH}, integration):[30] 9.73 (d, 5.7 Hz, 2), 7.89 (d, 8.1 Hz, 2), 7.08 (5.7 Hz, 2), 7.72−7.64 (m, 12), 7.53−7.47 (m, 50). ^{13}C NMR (CD_2Cl_2) (proton decoupled, shift (ppm), (multiplicity, J_{C-P})):[30] 156.5 (s), 155.9 (s), 155.6(s), 154.3 (s), 134.2 (d, 1.4 Hz), 134.2 (s), 132.4 (m), 129.8 (m), 128.0 (dd, 108.0 Hz, 1.7 Hz), 124.2 (s), 121.0 (s). IR (CH_2Cl_2 solution): 2085 (w), 2056 (s), 2045 (sh). The sample for elemental analysis was dried in vacuo at 150−160 °C. Anal. Calcd. for $(PPN)_2[Ru(bpy(CN)_4]\cdot 0.6H_2O$: C, 71.27; H, 4.81; N, 7.73. Found: C, 71.31; H, 4.55; N 7.36.

Gravimetric Measurements. General procedures have been previously described.[1−4] Samples of $(PPN)_2[Ru(bpy)(CN)_4]\cdot 4H_2O$ were obtained by drying more highly hydrated samples over anhydrous $CaSO_4$. Hydration measurements were made with an enclosed electronic balance (Mettler AE50). A reddish purple crystalline sample of $(PPN)_2[Ru(bpy)(CN)_4]\cdot 4H_2O$ (46.9 mg (0.0326 mmol)) was placed in a preweighed, clean, oven-dried porcelain crucible on the enclosed electronic balance pan. Beakers containing water and water-soaked glass wool to speed up the evaporation process were placed in the enclosed area. Over the next few hours, the sample gained an additional 6.3 mg as it gradually changed color from reddish

(13) Murphy, C. J.; Drane, W. D. *Proc. SPIE −Int. Soc. Opt. Eng.* **1995**, *2388*, 266.
(14) Bignozzi, C. A.; Chiorboli, C.; Indelli, M. T.; Rampi Scandola, M. A.; Varani, G.; Scandola, F. *J. Am. Chem. Soc.* **1986**, *108*, 7872.
(15) Winkler, J. R.; Creutz, C.; Sutin, N. *J. Am. Chem. Soc.* **1987**, *109*, 3470.
(16) Indelli, M. T.; Bignozzi, C. A.; Marconi, A.; Scandola, F. *Photochemistry and Photophysics of Coordination Compounds*; Yersin, H., Vogler, A., Eds.; Springer-Verlag: Heidelberg, 1987; pp 159−164.
(17) Scandola, F.; Indelli, M. T. *Pure Appl. Chem.* **1988**, *60*, 973.
(18) Kato, M.; Yamauchi, S.; Hirota, N. *J. Phys. Chem.* **1989**, *93*, 3422.
(19) Posse, M. E. G.; Katz, N. E.; Baraldo, L. M.; Polonuer, D. D.; Colombano, C. G.; Olabe, J. A. *Inorg. Chem.* **1995**, *34*, 1830.
(20) Waldhör, E.; Poppe, J. Kaim, W. *Inorg. Chem.* **1995**, *34*, 3093.
(21) Samuels, A. C.; DeArmond, M. K. *Inorg. Chem.* **1995**, *34*, 5548.
(22) Jiwan, J.-L. H.; Wegewijs, B.; Indelli, M. T.; Scandola, F.; Braslavsky, S. E. *Recl. Trav. Chim. Pays-Bas.* **1995**, *114*, 542.
(23) Timpson, C. J.; Bignozzi, C. A.; Sullivan, B. P.; Kober, E. M.; Meyer, T. J. *J. Phys. Chem.* **1996**, *100*, 2915.
(24) Rampi, M. A.; Indelli, M. T.; Scandola, F.; Pina, F.; Parola, A. J. *Inorg. Chem.* **1996**, *35*, 3355.
(25) (a) *Inclusion Compounds*; Atwood, J. L., Davies, J. E. D., MacNicol, D. D., Eds.; Academic Press: New York, 1984; Volume 2, pp 123−166. (b) MacNicol, D. D.; Wilson, D. R. *J. Chem. Soc., Chem. Commun.* **1976**, 494. (c) Hardy, A. D. U.; MacNicol, D. D.; Wilson, D. R. *J. Chem. Soc., Perkin Trans.* **1979**, *2*, 1011.
(26) Zelonka, R. A.; Baird, M. C. *Can. J. Chem.* **1972**, *50*, 3063.
(27) Bennett, M. A.; Smith, A. K. *J. Chem. Soc. Dalton Trans.* **1974**, 233.
(28) Robertson, D. R.; Robertson, I. W.; Stephenson, T. A. *J. Organomet. Chem.* **1980**, *202*, 309.
(29) Maruyama, M.; Matsuawa, H.; Kaizu, Y. *Inorg. Chim. Acta.* **1995**, *237*, 159.
(30) The chemical shifts depend on the concentration of the compound and water in the sample.

Table 1. Crystal Data, Data Collection, and Refinement Parameters for $(PPN)_2[Ru(bpy)(CN)_4]\cdot 2CH_3CN\cdot 2(CH''_3CH_2)_2O\cdot 2H_2O$

formula	$C_{98}H_{98}N_{10}O_4P_4Ru$	diffractometer	Siemens SMART Platform CCD
habit, color	platelet, violet	θ range, deg	0.93 to 25.03
size, mm	0.55 × 0.45 × 0.05	index ranges	$-26 < h < 25$, $0 < k < 14$, $0 < l < 38$
lattice type	monoclinic	reflections collected	44 174
space group	$P2_1/c$	unique reflections	15 335 ($R_{int} = 0.066$ 6)
a, Å	21.9047(5)	system used	SHELXTL-V5.0
b, Å	12.4506(3)	solution	direct methods
c, Å	32.1443(9)	refinement method	full-matrix least-squares on F^2
β, deg	94.958(1)	weighting factors,[a] a, b	0.039, 2.855
V, Å^3	8733.8(4)	absorption correction	SADABS[b]
Z	4	max., min. transmission	1.000, 0.736
fwt., g mol^{-1}	1704.89	data, restraints, parameters	15333, 0, 893
D_c, g cm^{-3}	1.296	R_1, wR_2 ($I > 2\sigma(I) = 11062$)	0.1108, 0.2581
μ, mm^{-1}	0.308	R_1, wR_2 (all data)	0.1379, 0.2713
$F(000)$	3568	goodness-of-fit (on F^2)	1.069
λ, Å	0.71073	largest diff. peak, hole, eÅ^{-3}	1.289, −1.339
T, K	173(2)		

[a] $w^{-1} = [\sigma^2(F_o^2) + (aP)^2 + (bP)]$, where $P = (F_o^2 + 2F_c^2))/3$. [b] Sheldrick, 1996.

purple to red burgundy and finally to orange before constant mass was reached. The total mass gain corresponds to a gain of 11 ± 1 equiv of water and a formulation of $(PPN)_2[Ru(bpy)(CN)_4]\cdot 15H_2O$ for the fully hydrated salt. Thermal dehydration experiments were performed by thermal gravimetric analysis (TGA) on a Perkin-Elmer TGA 7 under a nitrogen gas purge. Samples for the TGA experiments were prepared by grinding crystalline samples of the compound and exposing the resulting powder to 100% humid air for 15 h prior to the experiments. In a typical thermal scan, the instrument's pan was loaded with a fully hydrated sample of $(PPN)_2[Ru(bpy)(CN)_4]\cdot xH_2O$ (11.612 mg) at room temperature (20 °C); the temperature was increased at a rate of 5.0 °C per minute to 250 °C and it was observed that the water is lost in two steps; the first step begins at room temperature and the onset of the second step is at 60 °C. The final mass of the melted anhydrous material was 9.779 mg, corresponding to a total loss of 15 equiv of water.

In a second set of experiments, the temperature of a sample was kept at room temperature (20−22 °C) for 60 min prior to the temperature increase to study water desorption in nitrogen purge at ambient temperatures. In this case, a hydrated sample (9.171 mg) lost 1.049 mg (11 equiv) of water during the initial purge; the temperature was then increased at 5.0 °C per minute to 250 °C. Again the onset of the second dehydration step began at 60 °C; the anhydrous sample was produced by the loss of an additional 0.369 mg (4 equiv) of water.

Single-Crystal X-ray Data Collection. Violet crystals of X-ray quality were grown from acetonitrile solution with diethyl ether as a cosolvent by vapor diffusion. A platelet, 0.55 × 0.45 × 0.05 mm, was selected and attached to a glass fiber under a stream of cold nitrogen to minimize solvent loss. Due to the large channels present in these crystals (vide infra), the solvent molecules of crystallization escape from this compound rapidly. The structure reported here is based on the best of several data collections. The diffraction data were collected on a Siemens SMART system at 173 K.[31] An initial set of cell constants was calculated from reflections harvested from three sets of 20 frames. These initial sets of frames are oriented such that orthogonal wedges of reciprocal space were surveyed. This produces orientation matrixes determined from 96 reflections. Final cell constants are calculated from a set of 8192 strong reflections from the actual data collection. The data were collected by the hemisphere collection method, where a randomly oriented region of reciprocal space is surveyed to the extent of 1.3 hemispheres to a resolution of 0.84 Å. Three major swaths of frames are collected with 0.30° steps in ω. Further details of data collection are given in Table 1. All experimental data are provided as Supporting Information.

The space group $P2_1/c$ was determined on the basis of systematic absences and intensity statistics.[32] A successful direct-methods solution was calculated which provided most non-hydrogen atoms from the E-map. Several full-matrix least-squares/difference Fourier cycles were performed which located the remainder of the non-hydrogen atoms. All non-hydrogen atoms were refined with anisotropic displacement parameters unless stated otherwise. All hydrogen atoms were placed in ideal positions and refined as riding atoms with individual (or group if appropriate) isotropic displacement parameters.

The structure was found to contain two diethyl ether and two acetonitrile molecules per asymmetric unit. Additionally, two more lone heavy atoms were found. As no precautions were taken to exclude water from the solvents or the crystallization vessel, these lone heavy atoms are assigned as the oxygen atoms of water molecules. All of these solvent molecules were disordered to some degree. Attempts to refine the structure including all of the disordered solvent molecules gave $R_1 =$ 15.8%. Additional information about the disordered solvent pocket was obtained with PLATON/SQUEEZE.[33] No additional voids were located. The disordered solvent pocket consists of 710.2 e$^-$ and a volume of 2214.7 Å^3 (out of a total unit cell volume of 8733.8 Å^3). The original data were corrected for the disordered solvent and the structure was refined to give a final R_1 value of 11.08%. This final structure is consistent with a lattice that has a sieve like structure, where solvent molecules are loosely held in channels that border the cyanide ligands of the chromophore dianions and sheets of PPN^+ cations. A more detailed description is given below.

Preparation of Anhydrous Films of $(PPN)_2[Ru(bpy)(CN)_4]$. Films of a vapochromically active anhydrous form of $(PPN)_2[Ru(bpy)(CN)_4]$ were obtained by casting films from dichloromethane onto calcium fluoride plates. The plates were placed in a IR solution cell that was wrapped with heating tape. The samples were conditioned by heating to 100 °C for 10−20 min, while the cell was purged with nitrogen gas that was dried by condensation at liquid nitrogen temperatures,[34] cooled, and exposed to 100% relative humidity several times before the final drying. Samples were allowed to cool to room temperature under the dry nitrogen purge before the FT-IR or emission spectra were recorded. Subsequent spectral data (vide infra) suggests that this procedure was required to produce samples of the active anhydrous form of $(PPN)_2[Ru(bpy)(CN)_4]$. Heating much above 100 °C gave an anhydrous form that exhibits much slower hydration reactions. UV−vis absorbance spectra of the anhydrous form were recorded from films on quartz slides that were treated in the same fashion.

(31) Siemens SMART Platform CCD, Siemens Industrial Automation, Inc., Madison, WI.

(32) SHELXTL Plus V5.0, Siemens Industrial Automation, Inc., Madison, WI.

(33) Spek, A. L. *Acta Crystallogr.* **1990**, *A46*, C34.

(34) Very dry nitrogen was dried by condensing less volatile impurities at 77 K. See: Nelson, G. O. *Gas Mixtures, Preparation and Control*; Lewis Publishers: Chelsea, MI, 1992; p 267.

Infrared Absorption Changes with Humidity. The changes with humidity in the infrared region were recorded on a film cast from dichloromethane solution onto an ATR crystal and recorded as previously described.[1] Anhydrous samples of $(PPN)_2[Ru(bpy)(CN)_4]$ were obtained for these studies as described above; upon exposing these samples to 100% humidity, we obtained a continuous series of spectra that allowed us to use the spectral data analysis package SPECFIT[35] to fit the spectral changes and calculate the eigenspectrum for the intermediate.

UV−Vis/NIR Absorption and Emission Measurements. Films of $(PPN)_2[Ru(bpy)(CN)_4]\cdot xH_2O$ were spin-coated at 2000 rpm onto 0.9 × 2.5 × 0.1 cm quartz slides from a 15 mg/mL dichloromethane solution. Constant humidity atmospheres for the samples were created by slowly purging an appropriately saturated saltwater solution[36] with nitrogen, routing the humidified nitrogen purge gas into a quartz cuvette holding the sample slide. UV−vis absorption and emission spectra were recorded at room temperature with a Princeton Instruments ST130 UV−vis/NIR-sensitive LN/CCD spectrometer. The CSMA v2.6A and Winspec v1.6.1 software packages were used for acquiring the absorbance and emission spectra. A 75-W xenon arc lamp was used for the absorbance measurements. The emission spectra (front face detection) were collected while the samples were irradiated at 435.8 nm with the interference filtered output of a medium-pressure 175-W Hg/Na lamp. The samples had o.d.'s at 435.8 nm that typically ranged between 0.48 and 0.55 at the two humidity extremes. The emission spectra were corrected for grating efficiency and detector response.[37]

Results

Synthesis. The new compound, $(PPN)_2[Ru(bpy)(CN)_4]\cdot xH_2O$, was synthesized as outlined in Scheme 1 by

Scheme 1

$$[BzRuCl_2]_2 + 2bpy \xrightarrow[20-25\ ^\circ C,\ CH_3CH_2OH]{} 2[BzRu(bpy)Cl]Cl$$

$$[BzRu(bpy)Cl]Cl + 4KCN \xrightarrow[0-4\ ^\circ C,\ CH_3OH]{h\nu,\ N_2} K_2[Ru(bpy)(CN)_4] + Bz + 2KCl$$

$$K_2[Ru(bpy)(CN)_4] + 2PPNCl \xrightarrow[H_2O]{} (PPN)_2[Ru(bpy)(CN)_4] + 2KCl$$

methathesis of the potassium salt of the dianion in water. We also developed a new photochemical route to the potassium salt of this dianion that offers slightly improved yields and simplified workup over the original photochemical synthesis[14] and two thermal synthetic routes that have been reported since this work was started.[22,29]

Isolation of the water insoluble anhydrous $(PPN)_2[Ru(bpy)(CN)_4]$ compound was effected by filtration followed by recrystallization and drying (under vacuum at 110−112 °C). Unless heroic measures are taken to protect the anhydrous solid with scrupulously dry gas atmospheres at all times, the product so obtained has small, variable amounts of water ($x \leq 1$). Simple purging of more highly hydrated material ($x \geq 4$) with a dry nitrogen atmosphere at room temperature results in material with the formulation $(PPN)_2[Ru(bpy)(CN)_4]\cdot 4H_2O$. Simple melting point determination studies with hydrated material (to 260 °C) showed that several solid phases are formed before reaching the melting point (238−242 °C, sealed tube). No decomposition was observed; solution UV−vis, IR, and NMR spectra of the sample were identical before and after the melting point determination.

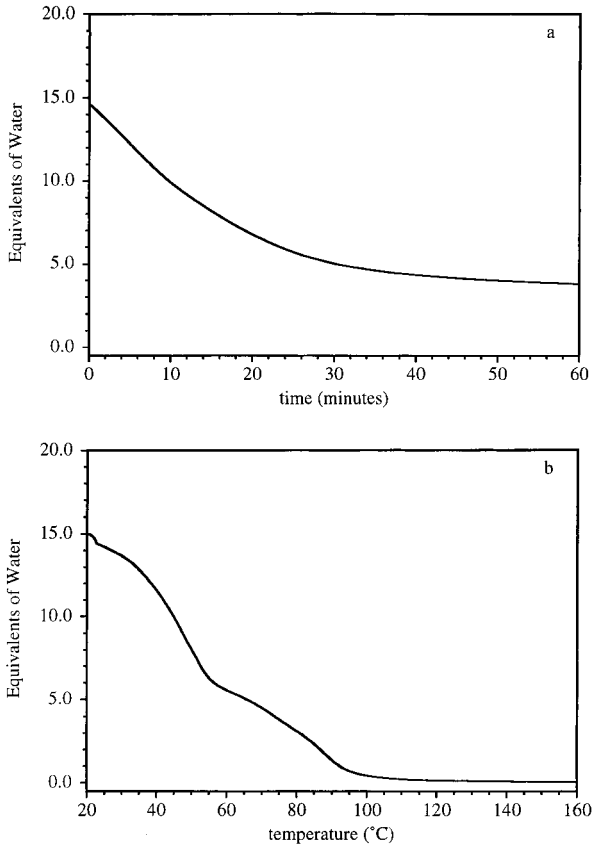

Figure 1. (a) Isothermal TGA trace for $(PPN)_2[Ru(bpy)(CN)_4]\cdot 15H_2O$ under a dry nitrogen purge and (b) TGA trace for $(PPN)_2[Ru(bpy)(CN)_4]\cdot 15H_2O$ heated at 5 °C/min.

Gravimetric Sorption Studies. The sorption properties of "dried" $(PPN)_2[Ru(bpy)(CN)_4]\cdot 4H_2O$ were investigated. Hydration of $(PPN)_2[Ru(bpy)(CN)_4]\cdot 4H_2O$ gave a mass increase that corresponds to 11 ± 1 equiv of water and a formulation of $(PPN)_2[Ru(bpy)(CN)_4]\cdot 15H_2O$ for the fully hydrated salt. More accurate measurements of the dehydration of hydrated samples were made by thermal gravimetric analysis (TGA). The fully hydrated samples that are yellow in color lost 11.0 ± 0.5 molecules of water per dianion to produce a red compound when the sample compartment was purged with dry nitrogen gas at ambient temperature (Figure 1a). An additional 4.0 ± 0.5 equiv of water were released when the temperature was increased to 100 °C to produce a purple solid. Additional heating (100 °C to 250 °C) caused no additional mass changes. A thermal scan starting with the 100% hydrated material under a nitrogen purge (Figure 1b) illustrates all of the mass losses, corresponding to a total of 15 ± 0.5 equiv, in a stepwise fashion, with the onset of the last step at 60 °C. After the thermal scan to 250 °C, the melted and

(35) Binstead, R. A.; Zuberbühler, A. D. *Specfit v2.09*; Spectrum Software Associates: Chapel Hill, NC, 1995.

(36) *The CRC Handbook of Chemistry and Physics*, 70th ed.; Weast, R. C., Ed.; CRC Press: Boca Raton, FL, 1990; p E43.

(37) The emission spectra were corrected to arbitrary units proportional to photons per energy for this calculation; see: Blasse, G.; Grabmeier, B. C. *Luminescent Materials*; Springer-Verlag: Heidelberg, 1994; p A225.

Table 2. Selected Bond Lengths (Å)[a] and Angles (deg)[a] for $(PPN)_2[Ru(bpy)(CN)_4]\cdot 2CH_3CN\cdot 2(CH''_3CH_2)_2O\cdot 2H_2O$

Ru(1)−C(12)	1.989(9)	C(11)−N(11)	1.127(9)	P(2)−C(39)	1.789(7)
Ru(1)−C(13)	2.011(8)	C(12)−N(12)	1.160(11)	P(2)−C(33)	1.825(7)
Ru(1)−C(11)	2.062(8)	C(13)−N(13)	1.124(10)	N(4)−P(4)	1.577(6)
Ru(1)−C(14)	2.071(8)	C(14)−N(14)	1.140(10)	N(4)−P(3)	1.593(6)
Ru(1)−N(2)	2.101(6)	N(3)−P(2)	1.575(6)	P(3)−C(63)	1.812(8)
Ru(1)−N(1)	2.116(6)	N(3)−P(1)	1.582(6)	P(3)−C(57)	1.814(8)
N(1)−C(1)	1.343(11)	P(1)−C(21)	1.788(7)	P(3)−C(51)	1.815(9)
N(1)−C(5)	1.350(10)	P(1)−C(27)	1.794(7)	P(4)−C(69)	1.782(7)
C(6)−N(2)	1.359(9)	P(1)−C(15)	1.821(7)	P(4)−C(81)	1.793(8)
C(10)−N(2)	1.347(10)	P(2)−C(45)	1.782(7)	P(4)−C(75)	1.808(7)
C(12)−Ru(1)−C(13)	91.9(3)	C(5)−N(1)−Ru(1)	116.5(6)	N(3)−P(2)−C(33)	115.0(3)
C(12)−Ru(1)−C(11)	89.5(3)	C(2)−C(1)−N(1)	125.0(9)	C(45)−P(2)−C(33)	106.4(3)
C(13)−Ru(1)−C(11)	89.4(3)	N(11)−C(11)−Ru(1)	176.3(6)	C(39)−P(2)−C(33)	106.8(3)
C(12)−Ru(1)−C(14)	89.7(3)	N(12)−C(12)−Ru(1)	176.9(7)	P(4)−N(4)−P(3)	137.8(5)
C(13)−Ru(1)−C(14)	87.9(3)	N(13)−C(13)−Ru(1)	171.7(7)	N(4)−P(3)−C(63)	108.6(4)
C(11)−Ru(1)−C(14)	177.2(3)	N(14)−C(14)−Ru(1)	178.4(8)	N(4)−P(3)−C(57)	109.6(4)
C(12)−Ru(1)−N(2)	173.5(3)	P(2)−N(3)−P(1)	138.7(4)	C(63)−P(3)−C(57)	107.0(3)
C(13)−Ru(1)−N(2)	94.4(3)	N(3)−P(1)−C(21)	109.4(3)	N(4)−P(3)−C(51)	115.5(4)
C(11)−Ru(1)−N(2)	92.2(2)	N(3)−P(1)−C(27)	113.3(3)	C(63)−P(3)−C(51)	107.6(4)
C(14)−Ru(1)−N(2)	88.9(3)	C(21)−P(1)−C(27)	108.4(3)	C(57)−P(3)−C(51)	108.2(4)
C(12)−Ru(1)−N(1)	96.8(3)	N(3)−P(1)−C(15)	108.7(3)	N(4)−P(4)−C(69)	116.2(4)
C(13)−Ru(1)−N(1)	171.3(3)	C(21)−P(1)−C(15)	107.4(3)	N(4)−P(4)−C(81)	107.1(4)
C(11)−Ru(1)−N(1)	91.1(2)	C(27)−P(1)−C(15)	109.5(3)	C(69)−P(4)−C(81)	107.3(4)
C(14)−Ru(1)−N(1)	91.7(3)	N(3)−P(2)−C(45)	107.3(3)	N(4)−P(4)−C(75)	111.0(3)
N(2)−Ru(1)−N(1)	76.9(3)	N(3)−P(2)−C(39)	111.0(3)	C(69)−P(4)−C(75)	106.4(3)
C(1)−N(1)−C(5)	116.7(7)	C(45)−P(2)−C(39)	110.3(3)	C(81)−P(4)−C(75)	108.6(3)
C(1)−N(1)−Ru(1)	126.7(6)				

[a] Estimated standard deviations in the least significant figure are given in parentheses.

refrozen compound is dark blue purple; it does not sorb water as readily as it did prior to the scan until it has been redissolved and precipitated. Anhydrous samples that have not been heated past 100 °C are readily able to regain the 15 waters of hydration. These data suggest that the anhydrous state produced by heating above 100 °C to remove the last four waters of hydration may have a different (and less permeable) crystal structure than the "low temperature material" with $0 \leq x \leq 15$.

Single-Crystal X-ray Structure of $(PPN)_2[Ru(bpy)(CN)_4]\cdot 2CH_3CN\cdot 2(CH_3CH_2)_2O\cdot 2\ H_2O$. Crystals suitable for an X-ray structure determination of solvated forms of $(PPN)_2[Ru(bpy)(CN)_4]$ grow quite readily from acetonitrile/ether solutions; however, both of these volatile solvents were included as guests in the lattice. Attempts to grow crystals from solvents with lower vapor pressures were unsuccessful. The mounting and transfer of a crystal was difficult because the crystals readily lost the solvent guests with an accompanying loss of single crystallinity. The partial loss of solvent produced crystals of relatively poor quality, especially with regard to the exact placement of the solvent molecules in the unit cell. The best structure we were able to obtain has a R_1 value of 11.08%, when the effects of disordered solvent of crystallization are minimized via a standard computational method[33] (vide supra). Nonetheless, the structure provides useful information as it shows the arrangement of the cations and anions in the cell. The position of these ions give a large solvent pocket in the unit cell. The unit cell contains eight acetonitrile, eight diethyl ether molecules, and eight single heavy atoms (most likely the oxygen of water molecules) in addition to the four dianions and eight cations. The volume occupied by these solvent molecules is approximately 25% of the total volume of the crystal! As illustrated in Figure 2, the hydrophobic PPN^+ cations form "sheets", in the *ab* plane, while the hydrophilic dianionic chromophores form stacks in the *a* direction of the structure. This creates solvent pockets that are

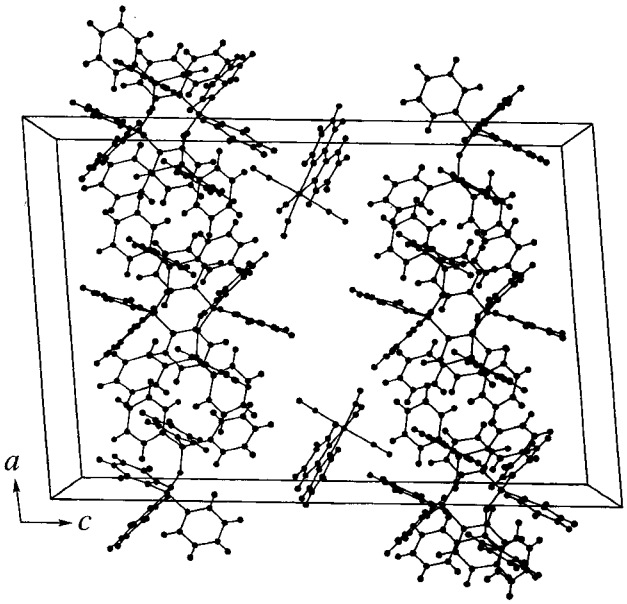

Figure 2. The projection of $(PPN)_2[Ru(bpy)(CN)_4]$ down the *b* axis onto the *ac* plane (solvent molecules are omitted from pocket for clarity).

located near the cyanide ligands of the dianion. These "pockets" align in the "*b*" direction of the lattice to form channels that guest molecules may go through when they are sorbed by the sample. Selected structural information is given in Table 2.

FT-IR Spectral Studies. Changes in the IR spectrum of solid $(PPN)_2[Ru(bpy)(CN)_4]\cdot xH_2O$ show that the water enters the crystal lattice as a guest. At low humidity, water interacts with the cyanide ligands of the dianion through the formation of hydrogen bonds. We observe that at room temperature under an atmosphere of pure nitrogen, a previously hydrated film of $(PPN)_2[Ru(bpy)(CN)_4]\cdot xH_2O$ still contains sorbed water. Careful heating of a sample to 100 °C removes these

Table 3. Selected Visible Absorption, Emission, and Infrared Spectral Changes as a Function of Relative Humidity

relative humidity (%)	λ_{max} (nm)			cyanide stretching frequencies ν (cm^{-1})[c]			
	absorption	emission[a]	IEI[b]	a_1	b_2	a_1'	b_1
dry N_2[d]	571	815	1.0	2083	2058	2050[e]	2041
N_2[f]	562	778	3.1	2083	2057	2053[e]	2041
11	517	735	4.9	2085	2056	2051[e]	2036
33	504	723	6.2	2086	2055	2044[e]	2036
52	484	690	9.6	2087	2054	2043[e]	2034
66	478	683	9.0	2087	2054	2043[e]	2034
79	470	681	8.6	2087	2054	2042[e]	2033
90	462	672	10.2	2086	2054	2042	2027
100	458	655	21.0	2086	2054	2042	2026

[a] The spectra were corrected for detector response and grating efficiency. [b] Integrated Emission Intensities were calculated from peak areas of photons per constant energy interval[37] plots and normalized to the spectrum obtained under a dry N_2 atmosphere. [c] Symmetry labels are assigned according to Cotton and Kraihanzel's method,[39] but using the coordinate system of Stufkens et al.[43] [d] Nitrogen purge gas and sample dried by methods described in the Experimental Section. [e] Obscured by the much stronger b_1 and b_2 stretches; peak positions were determined by spectral fits.[35] [f] Measurements made using nitrogen directly from a cylinder.

last traces of water. The intensity and area of the IR peaks associated with ν(O−H) at 3300−3500 cm^{-1} increase and the peaks shift to slightly lower energy when the rigorously dried sample is reexposed to humidity. These changes in ν_s(O−H) indicate increases in H-bonding between water molecules.[37] As seen in Figure 3a, significant shifts in the cyanide stretching region (1950−2150 cm^{-1}) are observed in conjunction with the sorption of water into a completely dry film. With the known dry and fully hydrated spectra of this series, we were able to use the factor analysis software package, SPECFIT,[35] to calculate the number of likely intermediates in the hydration process and their eigenspectra. This analysis is consistent with one intermediate. As seen in Figure 3b, most of the change in the cyanide region occurs between the dry and intermediate forms, while smaller shifts occur between the intermediate and fully exposed phases.

In the FT-IR study of discrete concentrations of water vapor, most of the change in the cyanide stretching region (1950−2150 cm^{-1}) occurs at low humidities, while much smaller shifts are observed at higher humidity levels; the changes are smaller and gradual with increasing humidity between 66 and 100% (Figure 4). These data are consistent with at least two hydration mechanisms and hydrogen-bonding modes. By curve fitting[38] the spectra, as summarized in Table 3, it becomes clear that certain ν(CN) stretching modes are affected more dramatically between 0 and 66% humidity than others by the presence of guest water molecules. The a_1 and b_2 CN stretching modes[39] (assigned to peaks at 2083 and 2058 cm^{-1}), that have large stretching components of the two axial cyanide ligands that are trans to each other, only shift slightly to (2087 and 2054 cm^{-1}); the a_1' and b_1 ν(CN) stretching modes, (assigned to a partially obscured peak at 2050 and a peak at 2041

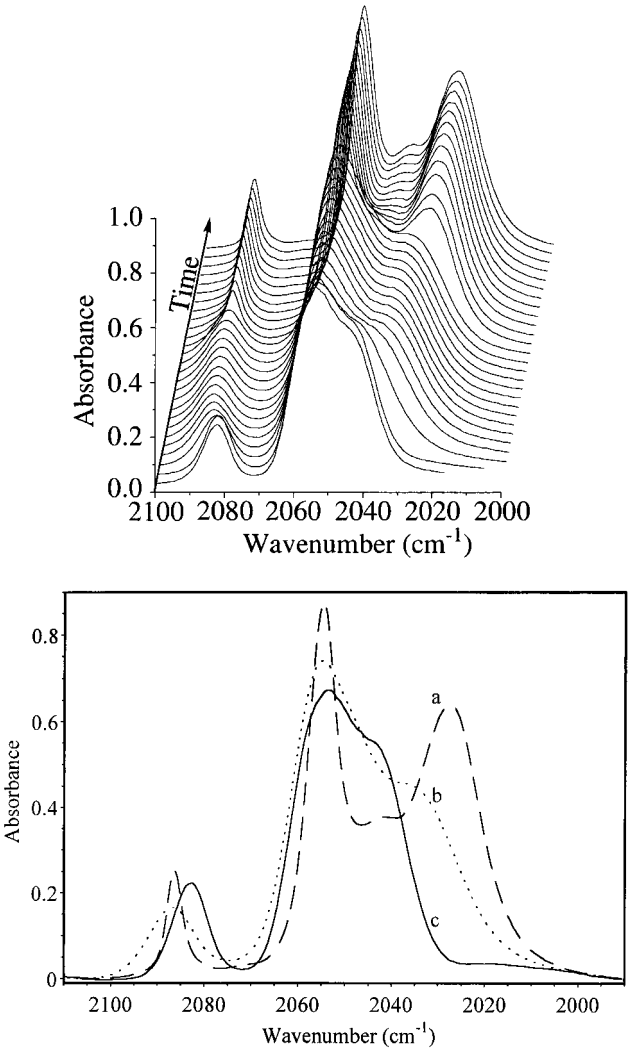

Figure 3. (a) Time-resolved (∼1 min apart) IR spectral changes during exposure of a rigorously dried film of $(PPN)_2$-$[Ru(bpy)(CN)_4]$ to 100% humidity. (b) "Eigenspectra" calculated from the IR spectra shown in part a: (a) fully exposed, (b) intermediate, and (c) dry.

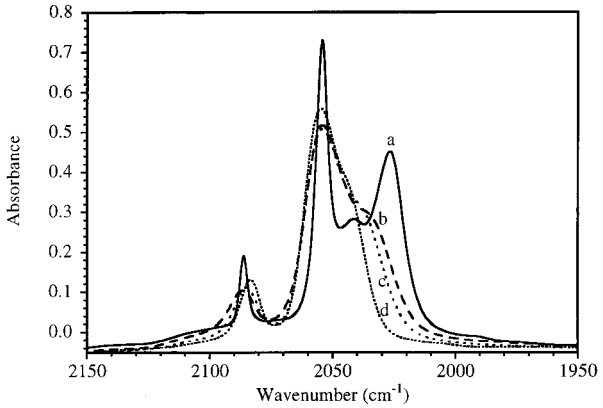

Figure 4. Solid-state FT-IR-ATR spectra of a film of $(PPN)_2$-$[Ru(bpy)(CN)_4]$ at different static relative humidities: (a) 100%, (b) 66%, (c) 15%, and (d) 0%.

cm^{-1}) associated with the two equatorial CN ligands trans to bpy shift to substantially lower energy (2043 and 2034 cm^{-1}) at low humidities, while the total area increases by ∼25%. These changes indicate that the CN triple-bond character of the cyanide ligands trans to bpy decrease at low relative humidity while the oscillator

(38) *Peaksolve for Microsoft Windows v1.05*; Galactic Industries: Salem, NH, 1996.

(39) Assignments of these bands are based on those made previously for *cis*-$M(CO)_4L_2$ complexes: Cotton, F. A.; Kraihanzel, C. S. *J. Am. Chem. Soc.* **1962**, *84*, 4432; our choice of coordinate systems interchanges *x* and *y*.

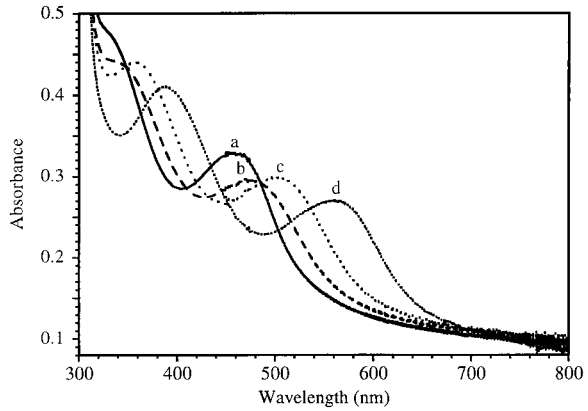

Figure 5. Solid-state UV−vis absorption spectra of a film of $(PPN)_2[Ru(bpy)(CN)_4]$ at different static relative humidities: (a) 100%, (b) 66%, (c) 15%, and (d) 0%.

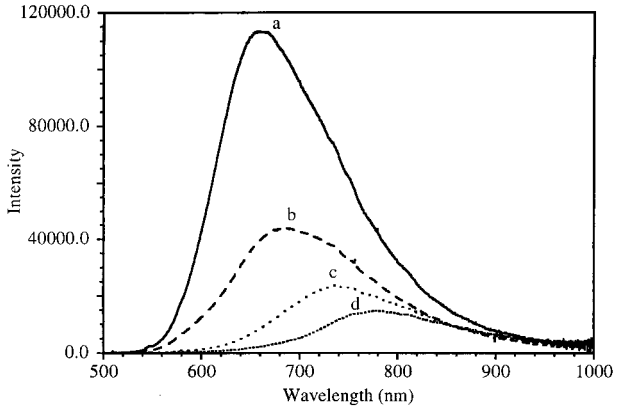

Figure 6. Solid-state emission spectra of a film of $(PPN)_2[Ru(bpy)(CN)_4]$ excited at 435.8 nm at different static relative humidities: (a) 100%, (b) 66%, (c) 15%, and (d) 0%.

strength of ν(CN) increases and is indicative of strong hydrogen-bonding interactions[40] between the water and cyanide ligands at low humidities.

The rise from 66% to 100% relative humidity shifts the a_1 and b_2 CN stretching modes only slightly from 2087 and 2054 cm^{-1} to 2086 and 2054 cm^{-1}. In this humidity range, the a_1' and b_1 ν(CN) stretching modes shift from 2043 and 2034 cm^{-1} to 2042 and 2026 cm^{-1}, while the total peak area remains constant. These changes are consistent with a further weakening of the cyanide ligands *trans* to bpy. As the oscillator strength remains unchanged, it is likely that these changes are due to a reorganization of the hydrogen bonding between water molecules, rather than the formation of new H-bonds to cyanide.

UV−Vis Absorption Studies. Solid samples of $(PPN)_2[Ru(bpy)(CN)_4]\cdot xH_2O$ exhibit a wide range of colors: from purple (dried by nitrogen purge) to yellow (exposed to water saturated nitrogen gas); these color changes were quantitatively monitored with UV−vis absorption spectroscopy. The lowest MLCT band[15,20,23] shifts 118 nm in total from 571 nm (dried nitrogen gas) to 458 nm (100% humidity). Between these two extreme conditions, various red and orange forms are observed with intermediate absorption maxima (Table 3). The largest λ_{max} shifts occur at low humidities where no significant changes in intensity are observed. The highly reproducible and reversible changes are complicated and not isosbestic over the entire humidity range. Several representative absorption spectra at different relative humidities are shown in Figure 5.

Emission Studies. The emission spectrum of $(PPN)_2[Ru(bpy)(CN)_4]\cdot xH_2O$ changes throughout the humidity range. Wavelength shifts, parallel to those observed in absorption, and intensity changes are also observed. For a scrupulously dry sample prepared by heating to 100 °C under rigorously dried nitrogen gas,[34] the emission is weak and occurs in the near-infrared spectral region (λ_{max} 815 nm). As the sample is exposed to higher concentrations of water vapor another peak grows in at higher energy. This peak, in the red region of the visible spectrum (λ_{max} 655 nm), continues to intensify with increasing relative humidity (Figure 6) up to about 52%. Eventually (after a slight decrease at 66% and 80%) as the relative humidity is increased still further (from 80% to 100%) the emission intensity more than doubles, but only small shifts in λ_{max} are observed. Quantitatively, the integrated peak area of the 100% humidity exposed sample is 21 times that of the 0% humidity exposed sample.[37] These changes are summarized in Table 3.

Discussion

Gravimetric and FT-IR studies unambiguously show that water molecules are sorbed from the gas phase as lattice guests in two processes the hydration processes exhibited by $(PPN)_2[Ru(bpy)(CN)_4]\cdot xH_2O$. The results of the single-crystal X-ray study of $(PPN)_2[Ru(bpy)(CN)_4]\cdot 2CH_3CN\cdot 2(CH_3CH_2)_2O\cdot 2H_2O$ show that a large pocket, capable of containing many water molecules, is present in the unit cell after the weakly held ether and acetonitrile molecules are released. We believe the mismatch of size, charge, and hydrophilicity of the PPN^+ and $[Ru(bpy)(CN)_4]^{2-}$ ions contributes to crystal lattice packing that produces these solvent pockets of considerable size and accessibility. It is likely that during hydration/dehydration cycles water molecules enter the lattice reversibly through channels along the "*b*" direction of the crystal. These channels account for 2218 $Å^3$ (~25%) of the unit cell volume. With the use of ice ($\rho_{ice} = 0.9168$ g/mL)[41] as a packing model for the waters of hydration, calculations suggest that the channel may hold up to 68 water molecules per unit cell (17 water molecules per dianion), in good agreement with gravimetric studies that show a total of 15 equiv of water per dianion are sorbed at 100% humidity.

Once the water molecules are in the channels that are produced by the crystal packing, they may interact directly with each other, with the $[Ru(bpy)(CN)_4]^{2-}$ chromophore or with the PPN^+ cations. A question of interest is the location of the water molecules in the lattice at low loadings of water (i.e. 0 to ~8) and whether they hydrogen bond to the cyanide ligands that are

(40) (a) Jeffrey, G. A. *An Introduction to Hydrogen Bonding*; Oxford University: Oxford, 1997; pp 220−225. (b) Pimentel, G. C.; McClellan, A. L. *The Hydrogen Bond*; W. H. Freeman: San Francisco, 1960; Chapter 3. (c) Joesten, M. D.; Schaad, L. J. *Hydrogen Bonding*; Marcel Dekker: New York, 1974; Chapter 3, pp 2−15, 195−239 (d) Vinogrado, S. N.; Linnell, R. H. *Hydrogen Bonding*; Van Nostrand Reinhold: New York, 1971.

(41) *The Merck Index*, 11th ed.; Budavari, S., Ed.; Merck & Co., Inc.: Rahway, NJ, 1989; p 9954.

oriented toward the channels. The gravimetric analyses indicate that the first 4 equiv of water that are sorbed by the anhydrous $(PPN)_2[Ru(bpy)(CN)_4]$ are held more tightly and can only be removed from the lattice by heating to 100 °C or under vacuum. A careful FT-IR study of the anhydrous $(PPN)_2[Ru(bpy)(CN)_4]$ and partially hydrated forms shows unambiguously that the initial waters of hydration are associated with hydrogen bonding to the cyanide ligands trans to bpy of the $[Ru(bpy)(CN)_4]^{2-}$ chromophore,[40] as the a_1' and b_1 stretching modes, that involve symmetric and asymmetric stretching motions of the equatorial cyanide ligands shift to substantially lower energies at low humidities (Table 3). These results suggest that the hydrogen-bonding interactions between water and $[Ru(bpy)(CN)_4]^{2-}$ are very strong at low water lattice loadings. It is particularly interesting that only small shifts to higher energy are observed in the stretching frequencies of the a_1 and b_2 modes attributable to the axial cyanides (CN_{ax}). These changes are consistent with weak hydrogen bonds to these CN_{ax} ligands, or they may be a result of induced effects transmitted through the CN_{eq} ligands. At relative humidities above 52% the changes in the ν(CN) region of the FT-IR spectrum are less dramatic. All the CN stretching modes shift to still lower energies, but the shifts are smaller than they are in the lower humidity range. These shifts are consistent with weakening of the CN triple bonds, both from increased back-bonding into the CN_{eq} π^* orbitals from the metal and from σ delocalization through hydrogen bonding with water. The calculated[35] intermediate spectrum from the time-resolved study for fully hydrating a completely anhydrous sample (Figure 3) resembles the FT-IR spectra recorded between static relative humidities of 52% and 79% relative humidity; this indicates that there is a change in mechanism of hydration in this region, which is also reflected by emission data.

The hydration-induced changes in the absorption and emission spectra may be interpreted with a clear picture of the structural and hydration features of the $(PPN)_2[Ru(bpy)(CN)_4]\cdot xH_2O$ system in hand. We adopt the axis system utilized by Lever et al., Stufkens, and tom Dieck et al. for studies of the related solvatochromic $W(CO)_4$-(α-diimine) systems[42−44] to aid the discussion. Briefly, this system orients the *z* axis on the 2-fold symmetry axis that bisects the angle between the two cyanide ligands trans to the bpy (equatorial CN, CN_{eq}); the *y* axis is aligned along the mutually trans cyanide ligands (axial CN, CN_{ax}). In this axis system, the labeling and ordering of the familiar pseudo-octahedral t_{2g} and e_g Ru d orbitals in the localized C_{2v} symmetry are $x^2-z^2(a_1) < yz(b_2) < xy(a_2) \ll xz(b_1) < y^2(a_1)$. The low lying Ru^{II}d-$\pi \rightarrow$ bpy-π^* MLCT transitions in this scheme (in order of increasing energy) are described as one electron excitations from $xy \rightarrow b_2$(bpy-π^*), $yz \rightarrow b_2$(bpy-π^*) and $x^2-z^2 \rightarrow b_2$(bpy-π^*), which are *x*, *z*, and *y* polarized, respectively. Of these three transitions, the $yz \rightarrow b_2$(bpy-π^*) is expected to be the most intense and the most sensitive to changes in the polarity of the surrounding medium.

Previously, λ_{max} absorption shifts of $[Ru(bpy)(CN)_4]^{2-}$ dissolved in various solvents have been found to correlate with a polarity index, the Gutmann solvent acceptor numbers.[23] Increases in the solvent polarity cause blue shifts in the aborption and emission bands. The details of the interaction mechanism in the cyanide system have been described in detail by Winkler,[15] Kaim,[20] and Meyer.[23] The two CN_{eq} ligands trans to bpy show enhanced π acceptor ability in more polar environments that stabilize the Ru(II) and lower the energy of the d_{xz} and d_{yz} orbitals. Slight increases in the excited-state energy may also occur. Both effects increase the (M)dπ−(bpy)π^* energy gap and cause the blue shift.

Our data show that absorption and emission shifts to the blue also result from varying the number of guest molecules within the crystal lattice that contains the $[Ru(bpy)(CN)_4]^{2-}$ anion. The largest wavelength shifts in the visible absorption and emission spectra at low humidities (0 to 66% relative humidity) coincide with the onset of significant changes in the ν(CN) region of the IR spectrum. These observations suggest that the large vapochromic shift in λ_{max} of this salt operates at low humidities via the formation of hydrogen bonds between water and the cyanide ligands of the chromophore. The initial hydrogen bonding between the first water molecules of hydration and the equatorial cyanide ligands located along the transition moment of the chromophore changes the dipole moment in the ground and excited states of the chromophore and the energy of the ruthenium-localized d_{xz} and d_{yz} orbitals. This type of hydrogen-bonding interaction should result in a smaller dipole moment for the chromophore and cause blue shifts in λ_{max}. The more polar CN_{eq} ligands transmit even slight changes in hydrogen bonding because they are trans to the weaker π-acceptor (bpy) and are along the MLCT transition dipole.

In addition to these blue shifts, a modest increase in emission intensity in the low humidity range is observed. It is likely that this increase results from the energy gap law,[45] as suggested by Bignozzi[14] or from exciting a different component of the MLCT when the absorption peaks have moved relative to the excitation wavelength.[43] At this time, we are unable to determine which possibility is correct.

In the high humidity regime (66−100% relative humidity) a large increase in the relative quantum yield of luminescence, smaller shifts in λ_{max} of the visible absorption and emission bands and a shift to lower frequencies of the a_1' and b_1 ν(CN) stretching modes occur. The IR changes indicate the additional water molecules slightly strengthen the previously formed H-bonding interactions. A likely mechanism for this second hydration is the oligomerization of additional water molecules to those hydrogen bonded to the equatorial cyanide ligands. In support of oligomerization we observe ν(O−H) IR peaks at 3300−3500 cm^{-1} increase in intensity and shift to slightly lower energy that have been previously been attributed to the formation of H-bonds between water molecules.[37] Oligomer-

(42) (a) Dodsworth, E. S.; Lever, A. B. P. *Inorg. Chem.* **1990**, *29*, 499. (b) Dodsworth, E. S.; Lever, A. B. P. *Coord. Chem. Rev.* **1990**, *97*, 271.

(43) Stufkens, D. J. *Coord. Chem. Rev.* **1990**, *104*, 39 and references therein.

(44) tom Dieck, H.; Renk, I. W. *Chem. Ber.* **1971**, *104*, 110.

(45) (a) Caspar, J. V.; Kober, E. M.; Sullivan, B. P.; Meyer, T. J. *J. Am. Chem. Soc.* **1982**, *104*, 630. (b) Caspar, J. V.; Meyer, T. J. *J. Phys. Chem.* **1983**, *87*, 952.

ization decreases the rate of the nonradiative decay processes of the chromophore by enhancing the rigidity of the hydrogen-bonding environment that occurs at high loading of the lattice or by shifting the deactivating nonemissive dd states to higher energy. In support of the first mechanism, the emission quantum yield of $Ru(bpy)(CN)_4]^{2-}$ in solution has recently been shown to increase when the anion is complexed by a macrocyclic ligand that efficiently forms several well-defined N−H···NC interactions.[24] Conversely the strong σ nature of the hydrogen-bonding interaction at the sp-hybridized nitrogen of cyanide affects the (M−L)σ and (M−L)σ^* energy levels much more than the π symmetry (M)dπ or (bpy)π^* orbitals. Although these σ and σ^* levels are not strongly involved in the MLCT electronic transitions observed directly in the emission and absorption spectroscopy, they are associated with the potentially deactivating dd states that could greatly affect the rate of nonradiative decay of the MLCT emission. In any event, emission lifetime studies as a function of relative humidity are planned to help sort out these possibilities.

Conclusions

The data presented show that solid $(PPN)_2[Ru(bpy)(CN)_4]$ reversibly senses the water vapor concentration in the surrounding atmosphere. Water molecules present in humid air are readily sorbed into the compound's sieve-like structure where they can interact with the chromophore. The vapochromic response of this compound over the 0−100% relative humidity range is the result of at least two mechanisms. The primary mechanism at low relative humidities gives rise to the impressive color change; it involves strong hydrogen-bonding interactions of the chromophore with the first water molecules that are sorbed into the crystal lattice. The second mechanism at high relative humidities is associated with smaller color changes but an impressive increase in the emission quantum yield; it is associated with filling the cavity with water molecules.

Acknowledgment. We are grateful to Dr. Victor G. Young Jr. and the X-ray crystallographic Laboratory at the University of Minnesota for the crystallographic work. This work has been funded by the INEEL University Research Consortium. The INEEL is managed by Lockheed Martin Idaho Technologies Co. for the U.S. Department of Energy, Idaho Operations Office, under contract number DE-AC07-94ID13223. The FT-IR spectrometer was purchased with funds from NSF Grant CHE-9307837.

Supporting Information Available: Details of the X-ray crystal structure of $(PPN)_2[Ru(bpy)(CN)_4]\cdot 2CH_3CN\cdot 2(CH_3CH_2)_2O\cdot 2H_2O$ including tables listing atomic coordinates, isotropic and anisotropic displacement parameters, torsion angles, hydrogen coordinates and anisotropic displacement parameters, bond lengths, bond angles, structure factors (calculated and observed), and CIF file (; and four figures including ORTEP drawing (with labeling scheme), FTIR-ATR spectra in the OH stretching region, unit cell projection on the *ab* plane and unit cell projection on the *bc* plane. This material is available free of charge via the Internet at http://pubs.acs.org.

CM980323I